Electronic Supplementary Information

Photonic-plasmonic resonator for SERS biodetection

Zheng Tian, Zhonghai Zhang*

Shanghai Key Laboratory of Green Chemistry and Chemical Processes, School of Chemistry and Molecular Engineering, East China Normal University, Shanghai 200241, China

*E-mail: zhzhang@chem.ecnu.edu.cn

Table of contents of supplementary information:

3. Additional references

1. Experimental section

1.1. Materials

The titanium foil (purity of 99.6%) with thickness of 0.1 mm was purchased from Jinjia Metal, China. Ethylene glycol (EG), ammonia fluoride (NH_4F), phenylalanine, glucose and riboflavin were purchased from Macklin Chemical and used as received. All aqueous solutions were prepared using deionized water (DI) with a resistivity of 18.2 MΩ cm at 25 °C.

1.2. Instruments.

The morphologies of samples were characterized by scanning electron microscopy (SEM, S4800, Hitachi) and high-resolution transmission electron microscopy (HRTEM, JEOL JEM 2100). The diffuse reflectance UV-vis adsorption spectra were recorded on a spectrophotometer (Shimadzu, UV 3600), with fine $BaSO_4$ powder as reference. The Raman spectra was measured through a confocal micro-Raman spectrometer (Renishaw-inVia Reflex) with excitation from a 785 nm laser. Photoelectron Spectroscopy (XPS) data were collected by an Axis Ultra instrument (Kratos Analytical) under ultrahigh vacuum ($<10^{-8}$ torr) and using a monochromatic Al Kα X-ray source operating at 150 W. The UPS measurements were conducted in an ultrahigh vacuum surface analysis system equipped with SCIENTA R3000 spectrometer with a base pressure of 10^{-10} mbar. Incident photon to current conversion efficiency (IPCE) of the Au/TiO_x were evaluated with a three-electrode system, which used the Au/TiO_x, Pt foil, and Ag/AgCl as working, counter, and reference electrodes, respectively, in a supporting electrolyte of Na_2SO_4 (0.1 M) solution.

1.3. Raman measurements

To study the SERS of these Au/TiO_x, a confocal micro-Raman spectrometer (Renishaw-inVia Reflex) is used as the measuring instrument. In all SERS tests, unless specifically stated, the excitation wavelength is 785 nm. The SERS spectra were

obtained with 10 s acquisition time unless specified. A series of standard solution of R6G with concentrations of 10^{-5}-10^{-12} M were used probe molecules. In each SERS measurements, 10 μL probe solution was dropped on the Au/TiO_x substrates followed by a gentle dry process.

1.4. Serum samples

A total of 56 blood serum samples were collected from 16 healthy volunteers (N), 21 LC, 19 PC patients with confirmed clinical diagnosis from Shanghai Cancer Center. All these samples were collected from each study subject between 6:00 and 8:00 a.m. after 12 h of overnight fasting. Prior to SERS measurement each sample was centrifuged at 3000 rpm for 10 min and the supernatant was obtained and stored in a freezer at -80 ℃

1.5. Enhanced factor calculation.

The Raman enhancement factors (EFs) were calculated according to the equation:

$$EF = (I_{SERS}/N_{SERS})/(I_{bulk}/N_{bulk}) \quad (1)$$

Where I_{SERS} and I_{bulk} are the Raman intensities in the SERS experiments and the normal Raman spectra (NRS) of R6G, respectively. N_{SERS} and N_{bulk} correspond to the number of probe molecules excited in the SERS and NRS tests. Here we use two Raman scattering peaks, R_1 at 612 cm^{-1} and R_3 at 1364 cm^{-1} were selected for the calculations of the EF. For comparison, the peak intensities of the bulk R6G directly placed on bare glass slide were detected as NRS data. To decrease the measuring error, the intensities were obtained by continually ran the test procedure at randomly selected 20 points and took the average. The Raman 1364 cm^{-1} intensity of Au NPs/TiO_x (1×10^{-12} M) is 252 counts with 10 s acquisition time, and that of bluk R6G is 452 counts with 0.5 s acquisition time. The Raman intensity ratio is estimated to be I_{SERS}/I_{bulk} = (252/10)/(452/0.5) = 2.79×10^{-2}.

$$N_{SERS} = N_A c V S_{Irr}/S_{dif} \quad (2)$$

In our SERS experiments, the dye solution with 10 μL volume was drop-casted on the SERS material with ~0.09 cm^2 substrate area followed by a gentle dry process. In N_{SERS}, where C is the dye concentration (1×10^{-12} M), V is the dye droplet volume (10 μL), N_A is the Avogadro constant, S_{Irr} is the laser spot area, and S_{dif} is the substrate area. To obtain the N_{bulk}, the high concentration (0.1 M) R6G solution (with sufficient volume) was drop-casted onto the bare glass. The bulk R6G crystals (thickness is larger than the laser penetration depth) were formed when the solution was dried out. Hence, we could use the density of R6G to calculate the number of molecules.

$$N_{bulk} = \rho S_{Irr} h N_A/M \quad (3)$$

Where ρ is the density of bulk dye (1.15 g/cm^3 for R6G), h = 29 μm is the laser penetration depth, and is the molar mass of dye (479.02 g/mol for R6G). Taking all the above-mentioned factors into account, the EF in the Au/TiO_x measurements can be derived as:

$$EF = \frac{I_{SERS}}{I_{bluk}} \times \frac{\rho h S_{dif}}{cVM} = 2.79\times 10^{-2} \times \frac{1.15\times 29\times 10^{-4}\times 0.09}{1\times 10^{-12}\times 10\times 10^{-6}\times 479.02} = 1.75\times 10^{9} \quad (4)$$

2. Supplementary Figures and Tables

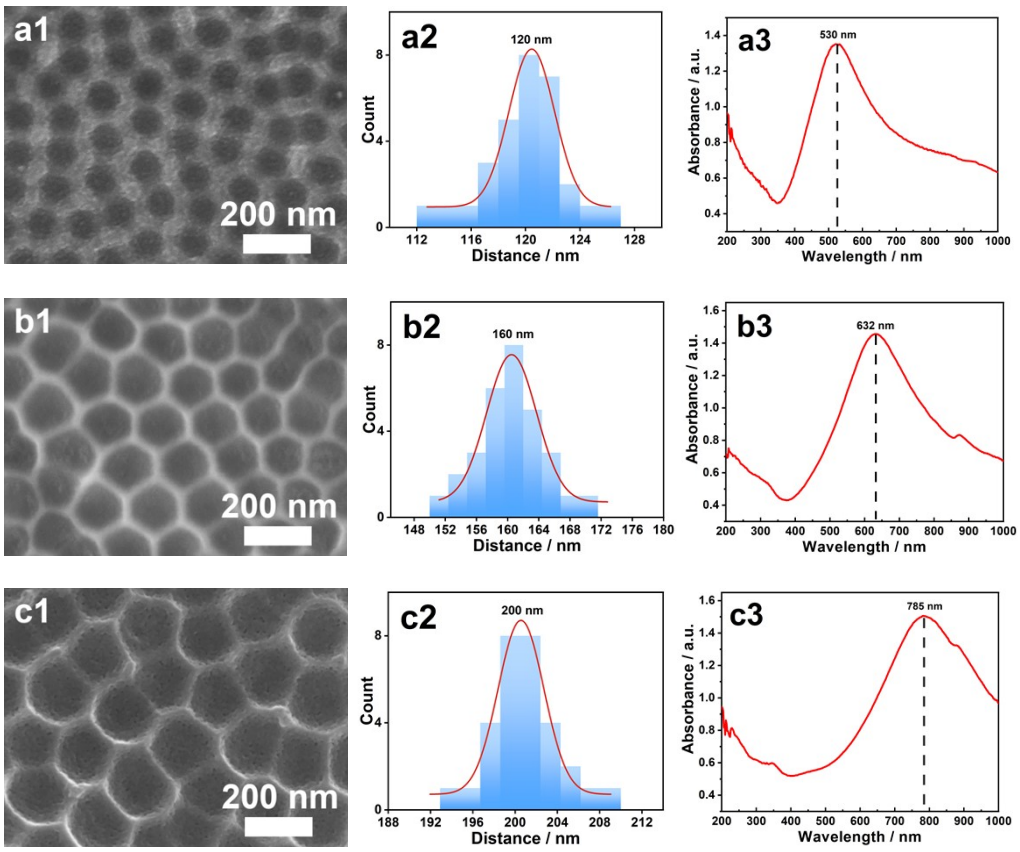

Fig. S1. The morphologies，size and optical properties of TiO_x nanocavities with different size and resonance wavelengths.

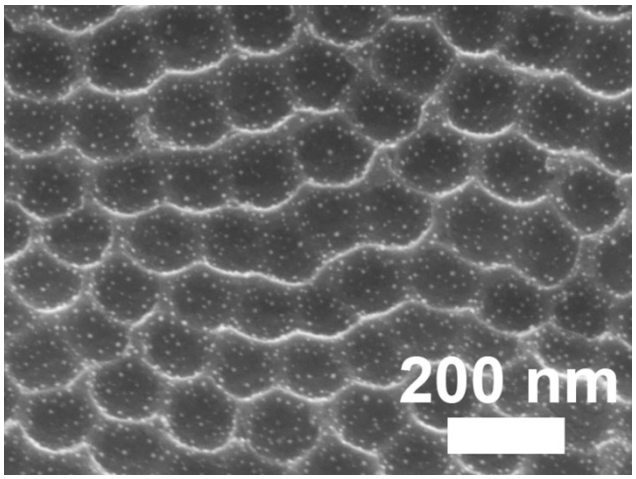

Fig. S2. SEM image of Au/TiO_x with sputtering time of 10 s.

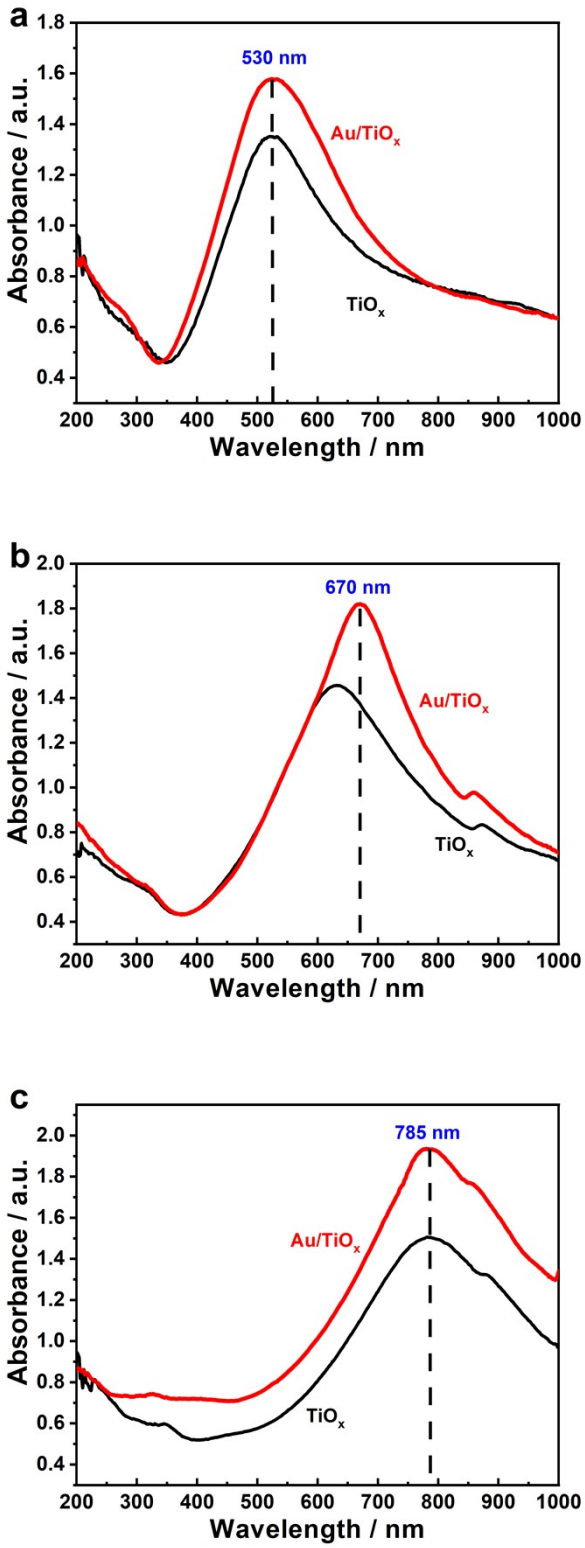

Fig. S3. Photonic-plasmonic resonators with different matched resonance wavelengths.

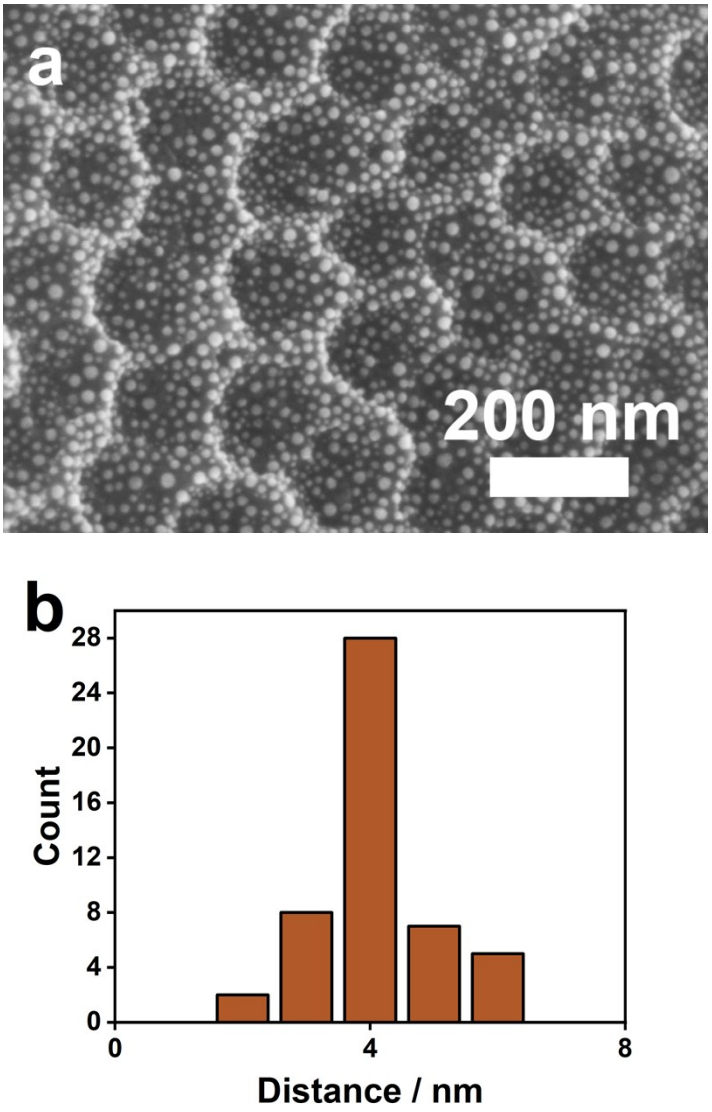

Fig. S4. (a) The high-power SEM images of Au/TiO_x with sputtering time of 30 s (b) distance between the Au nanoparticles.

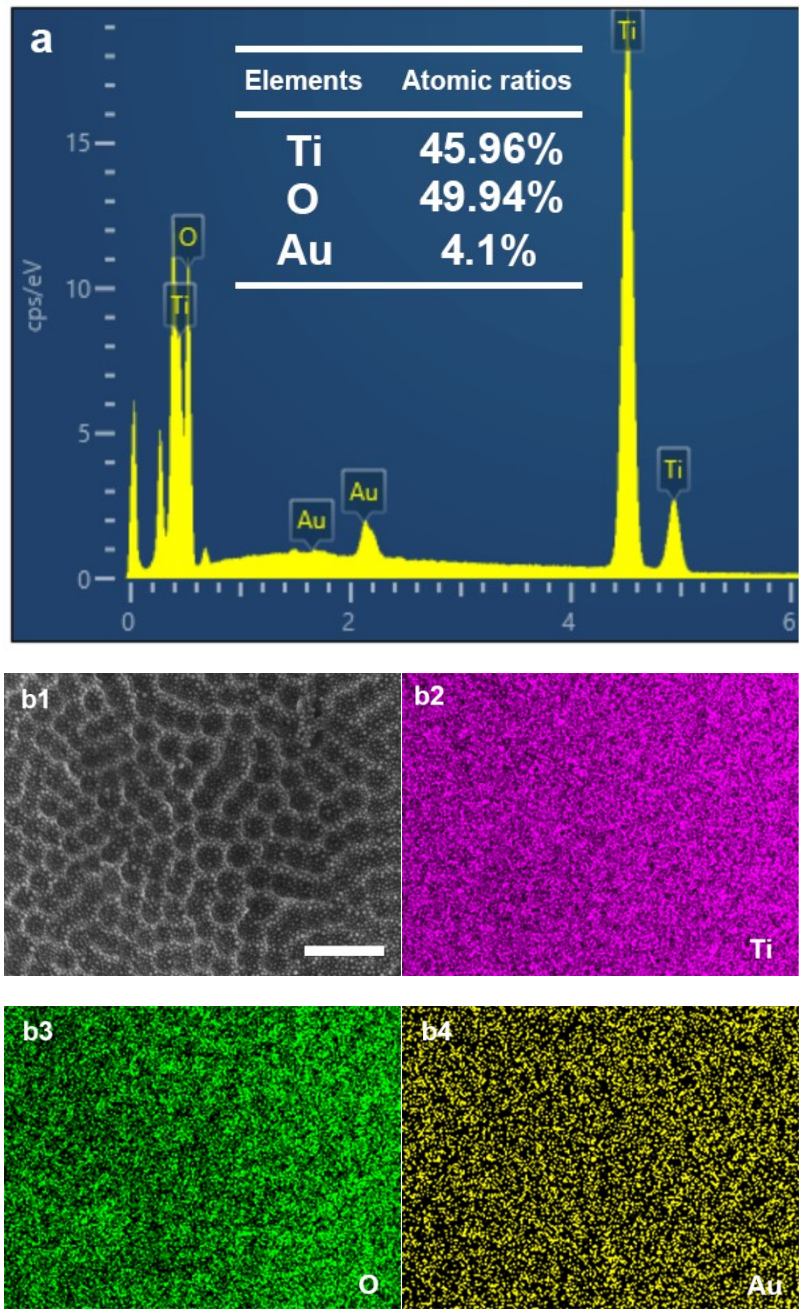

Fig. S5. (a) EDS curve and (b) EDS mapping images of Au/TiO_x with sputtering time of 30 s, the scale bar is 500 nm.

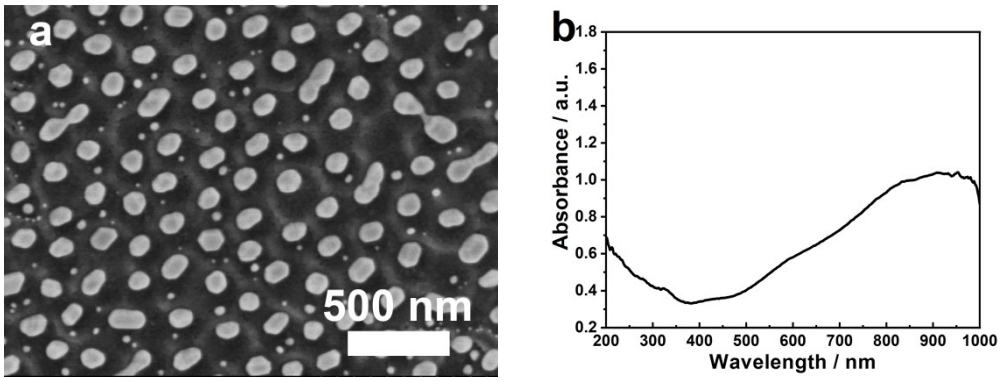

Fig. S6. (a) SEM image and (b) optical absorption of Au/TiO_x with sputtering time of 60 s.

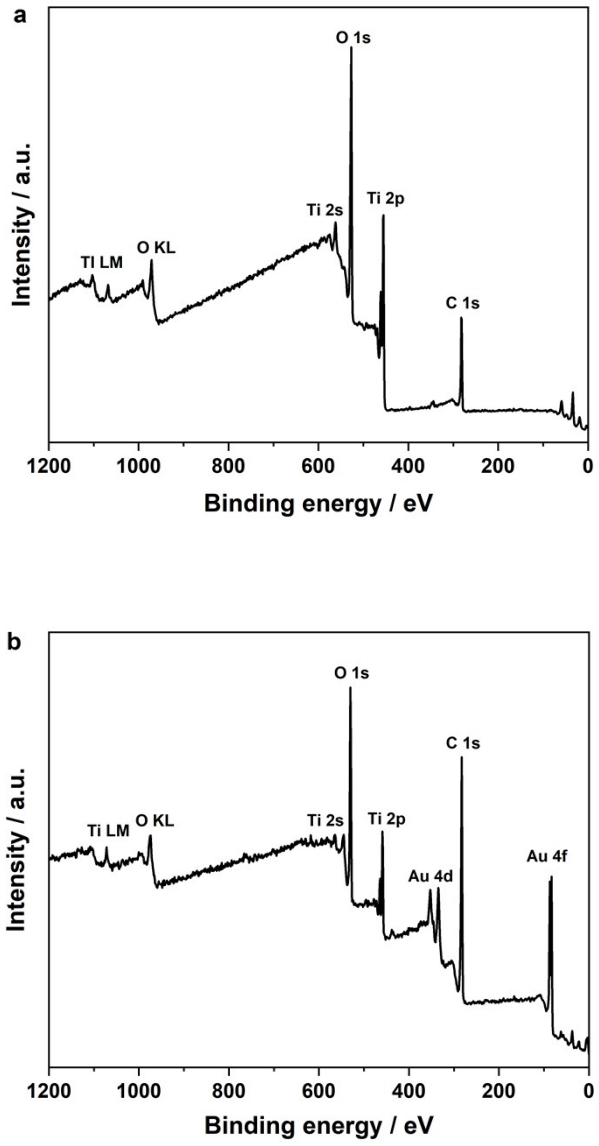

Fig. S7. XPS survey of (a) TiO_x and (b) Au/TiO_x.

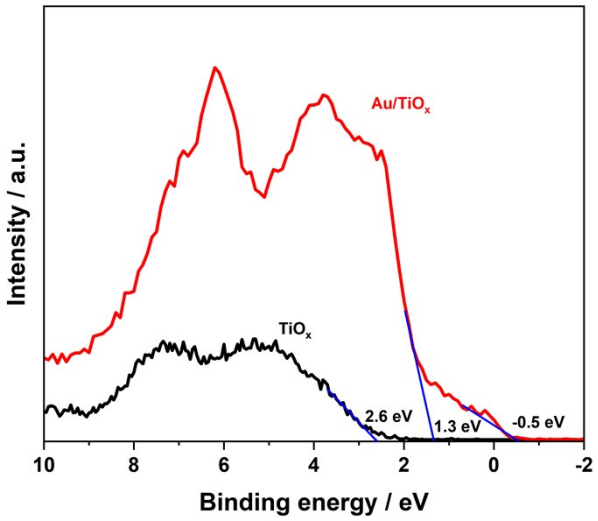

Fig. S8. XPS of valence band of TiO_x and Au/TiO_x.

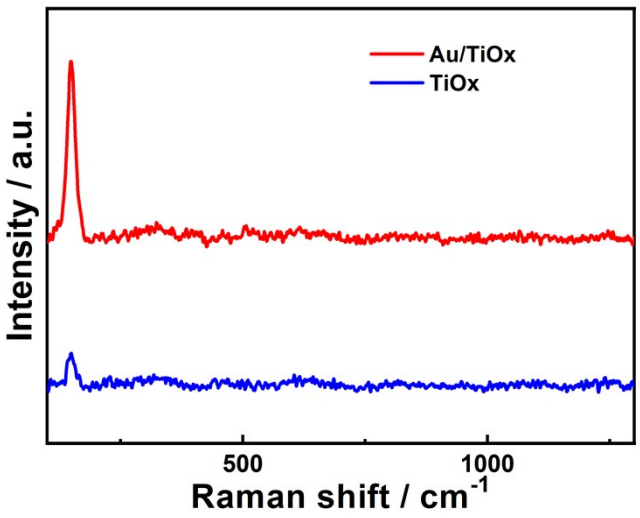

Fig. S9. Raman spectra of TiO_x and Au/TiO_x.

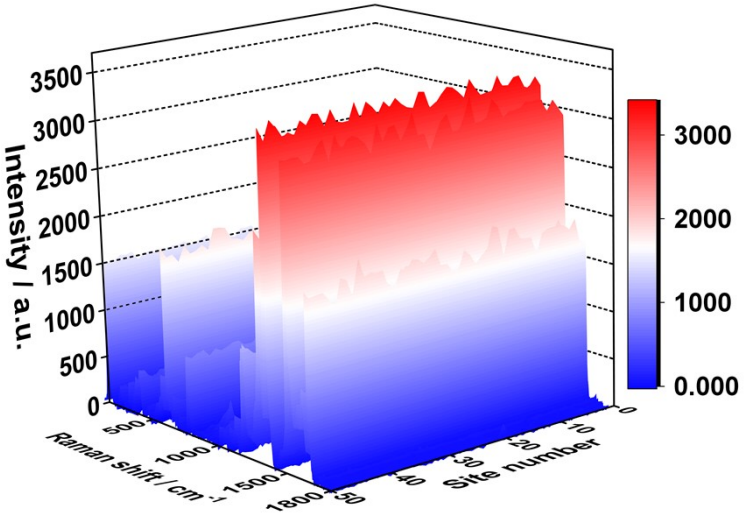

Fig. S10. 3D Raman spectra of 50 sites on one Au/TiO_x substrate.

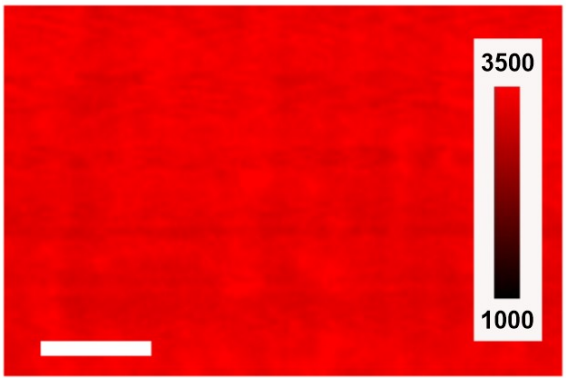

Fig. S11. The SERS mapping at 1364 cm^{-1} of 3000 sites, the scale bar is 10 μm.

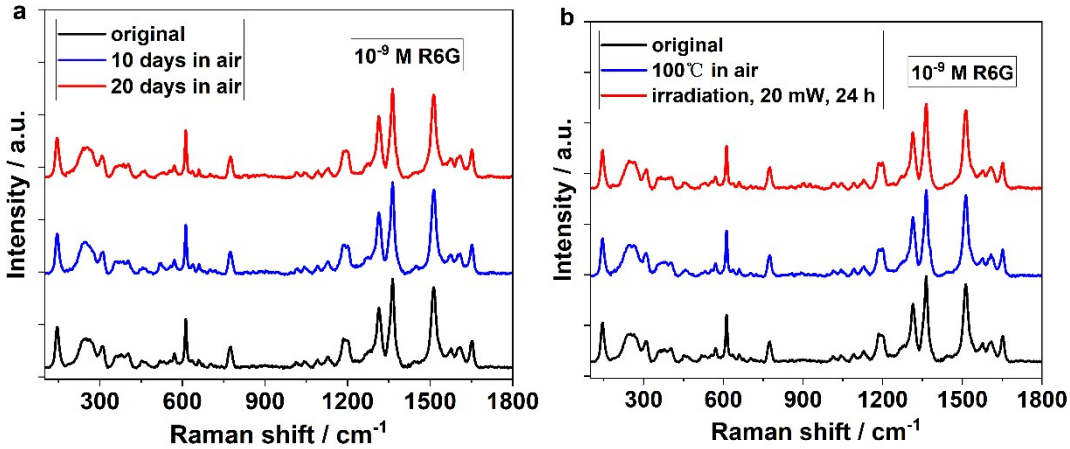

Fig. S12. The SERS detection stability of the substrates under (a) long-term preservation in air and (b) after being heated in air and irradiated by laser.

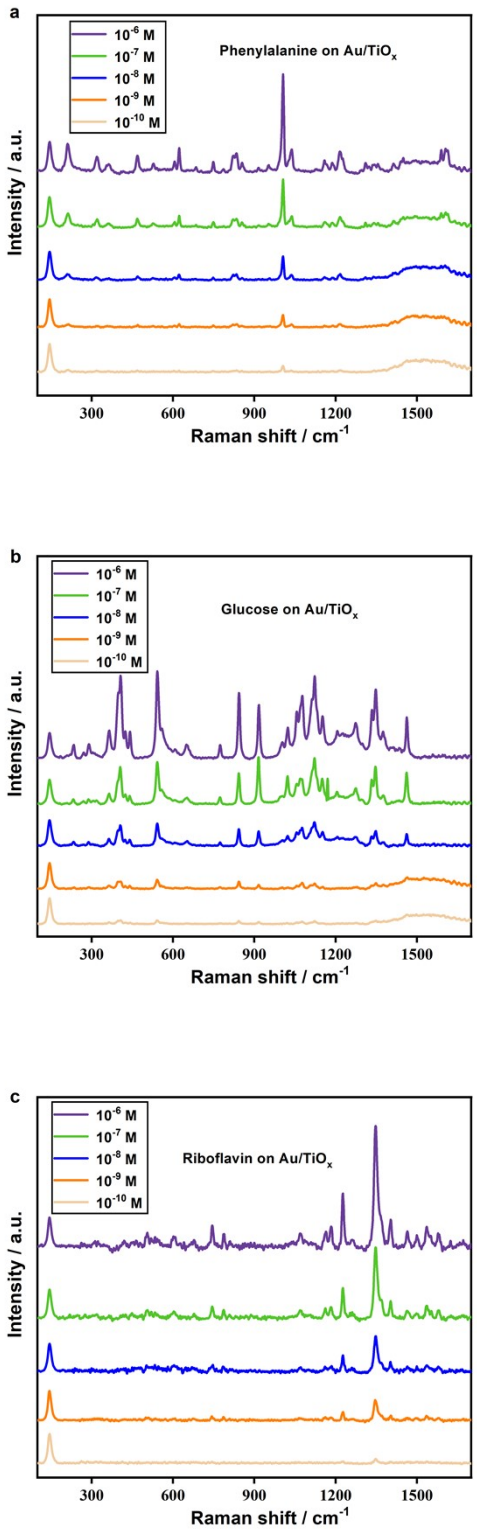

Fig. S13. the SERS spectra of biomolecules including (a) phenylalanine, (b) glucose and (c) riboflavin with different concentrations measured on the photonic-plasmonic resonator.

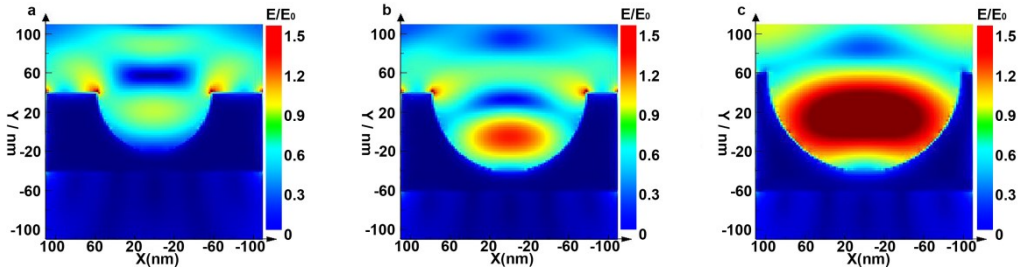

Fig. S14. FDTD simulation of photonic resonator with different size of nanocavity of (a) 120 nm, (b) 160 nm, (c) 200 nm.

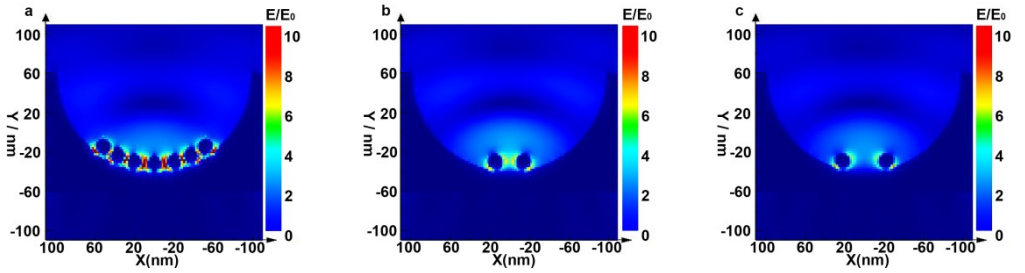

Fig. S15. FDTD simulation of (a) multiple Au nanoparticles with a separation of 4 nm in the nanocavity, (b) two Au nanoparticles with a separation of 20 nm and (c) 30 nm in the nanocavity.

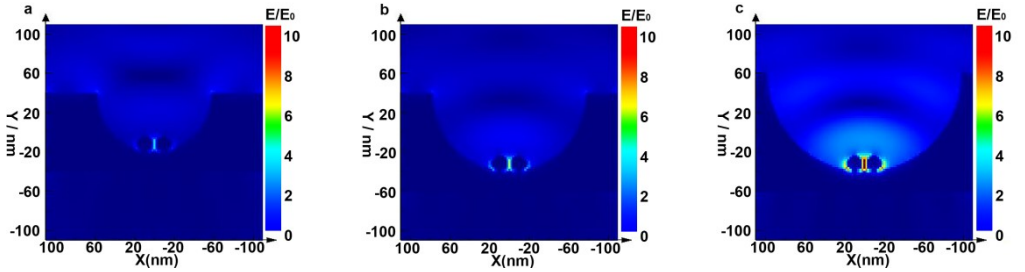

Fig. S16. FDTD simulation and SERS spectra of the photonic-plasmonic resonator with different size of nanocavity. Size of nanocavity of (a) 120 nm, (b) 160 nm, (c) 200 nm.

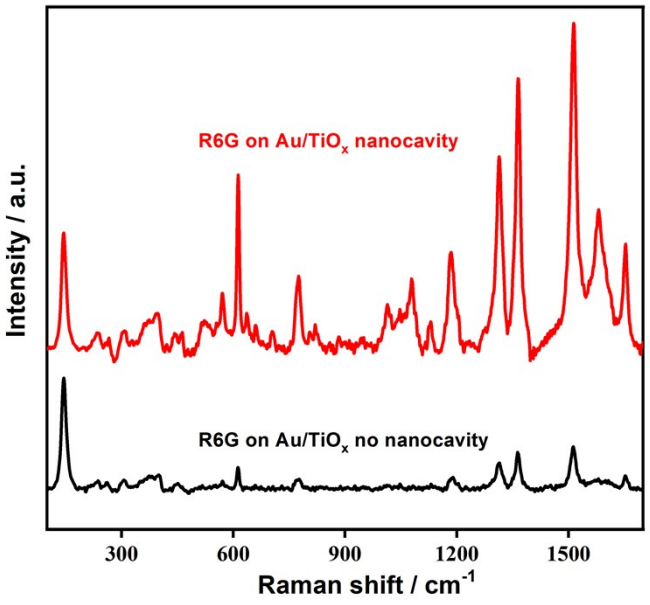

Fig. S17. Comparison of SERS signals of R6G on Au/TiO_x nanocavity and Au/TiO_x no nanocavity.

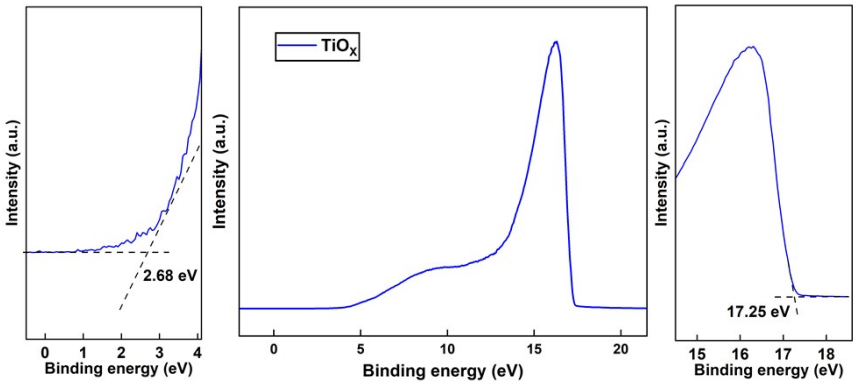

Fig. S18. UPS spectra of TiO_x.

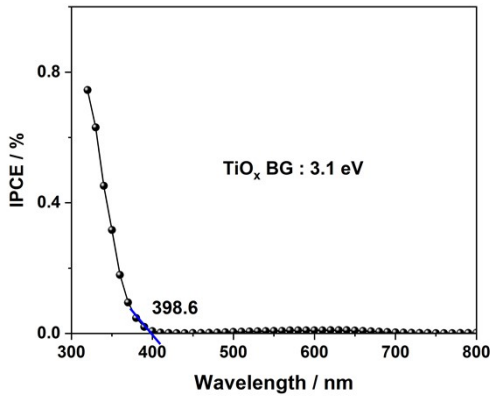

Fig. S19. IPCE plots of TiO_x.

To illustrate energy band structures of TiO_x, the band gap should be estimated, which is usually obtained from the optical absorption spectrum. Meanwhile, the unique nanocavity of TiO_x exhibited strong structural light absorption, masking the intrinsic photonic absorption activity. Therefore, the incident-photon-current-efficiency (IPCE) spectra were plotted and used to obtain the intrinsic threshold of photonic absorption.

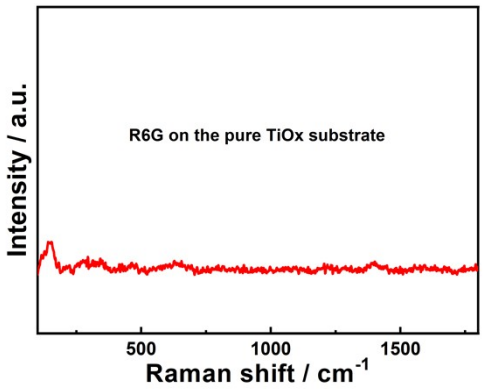

Fig. S20. Raman signal of R6G on the pure TiO_x substrate.

For TiO_x, 785 nm excitation light cannot excite TiO_x to generate electron-hole pairs, because the band gap of TiO_x is about 3.1 eV, larger than the photon energy of 785 nm excitation light (1.58 eV). In addition, 785 nm excitation light cannot excite R6G to produce carriers, because the energy of 1.58 eV is lower than the band gap of R6G molecule (2.3 eV). These results indicate that in the TiO_x/R6G structure, the charge transfer from TiO_x to the LUMO level of R6G, and from the HUMO level of R6G to TiO_x, which causes the SERS activity, cannot be achieved. Therefore, no Raman signal of R6G molecule was detected on the pure TiO_x substrate.

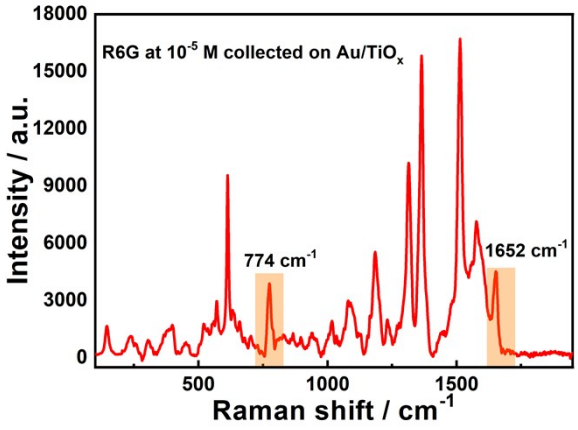

Fig. S21. Raman spectra of R6G at 10^{-5} M collected on Au/TiO_x substrate.

Calculation details for degree of CT

The calculation of CT degree (ρ_{CT}) is based on the well-established method in previous publications. The CT degree is calculated as follows:

$$\frac{I^K(CT) - I^K(SPR)}{I^K(CT) + I^0(SPR)}$$

In the spectral region shown in Fig. S21, two different bands were selected, namely the totally symmetric band 774 cm^{-1} and the non-totally symmetric band 1652 cm^{-1}. Among them, only SPR contributed to SERS signal in the totally symmetric band, whose intensity was denoted as I^0(SPR), while another band that was non-totally symmetric was denoted as I^k(CT). I^k(SPR) is the measured intensity in the region of the spectrum, it is normally approaches or goes to zero. Based on the above, the contribution degree of CT mechanism to SERS effect was 0.46.

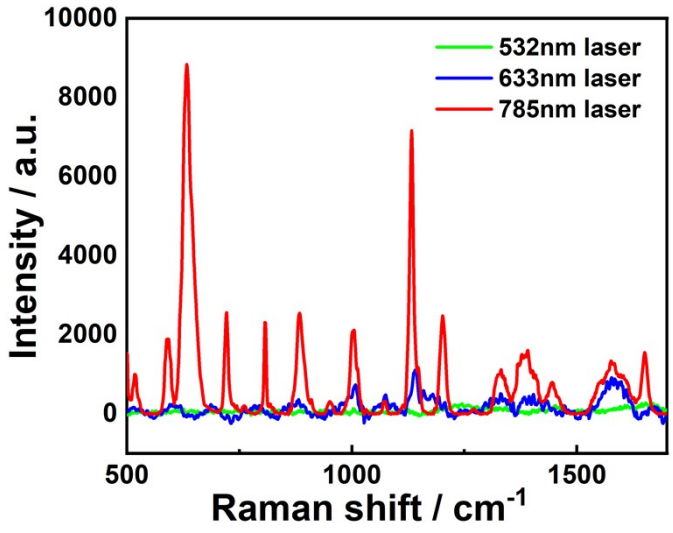

Fig. S22. Comparison of cancer serum samples under different lasers on the photonic-plasmonic resonator substrate.

Table S1. Comparison of semiconductor SERS substrates for enhancement of non-resonant molecules.

Material	Probe molecule	EF	Reference
Ag/Ag-doped TiO_2	4-MBA	1.68×10^6	[1]
Cds nanoparticles	4-Mpy	10^2	[2]
Amorphous TiO_2	4-MBA	1.86×10^6	[3]
ZnO superstructure	4-MPY	10^5	[4]
ZnO	4-MBA	6.9×10^6	[5]
ZnO nanosheets	4-Mpy	7.7×10^5	[6]
Au@$CsPbBr_3$	R6G	5.9×10^6	[7]
Fe_3O_4@GO@TiO_2	CuPc	8.0×10^6	[8]
Cu_2O	R6G	8×10^5	[9]
Amorphous ZnO nanocage	4-MBA	6.6×10^5	[10]
$MAPbCl_3$ single crystal	4-MPY	2.6×10^5	[11]
WN/C hybrid nanobelts	BPA	6.5×10^8	[12]
Au NPs/TiO_x	R6G	1.75×10^9	This work

Table S2. Serum SERS peak positions and vibrational mode assignments.

Peak position/cm^{-1}	Vibrational mode	Major assignments
491	Ring vibration	L-Arginine
590	N/A	Amide VI
633	C–S stretching	L-Tyrosine
722	C–H bending	Hypoxanthine
808	C–C–O stretching	L-Serine
888	C–O–H twist vibration	D-Galactosamine
950	C–H bending	Hypoxanthine
1004	C–C symmetric stretch	Phenylalanine
1071	C–N stretching	Collagen
1132	C–N stretching	D-Mannose
1201	Ring vibration	Tryptophan
1270	N/A	Amide III
1331	C–H stretching	Nucleic acid bases
1390	Ring vibration	Tryptophan
1444	H–C–H stretching	Collagen, phospholipids
1577	C=C stretching	phenylalanine, acetoacetate, riboflavin

1670	C=O stretching	Collagen, α-Helix

3. Supplementary References

[1] L. Zhou, J. Zhou, W. Lai, X. D. Yang, J. Meng, L. B. Su, C. J. Gu, T. Jiang, E. Y. B. Pun, L. Y. Shao, L. Petti, X. W. Sun, Z. H. Jia, Q. X. Li, J. G. Han, P. Mormile, Irreversible accumulated SERS behavior of the molecule-linked silver and silver-doped titanium dioxide hybrid system, Nat. Commun. 11 (2020) 1785.

[2] D. Qi, L. Lu, L. Wang, J. Zhang, Improved SERS Sensitivity on Plasmon-Free TiO2 Photonic Microarray by Enhancing Light-Matter Coupling, J. Am. Chem. Soc. 136 (2014) 9886.

[3] X. Wang, W. Shi, S. Wang, H. Zhao, J. Lin, Z. Yang, M. Chen, L. Guo, Two-Dimensional Amorphous TiO2 Nanosheets Enabling High-Efficiency Photoinduced Charge Transfer for Excellent SERS Activity, J. Am. Chem. Soc. 141 (2019) 5856.

[4] R. Haldavnekar, K. Venkatakrishnan, B. Tan, Non plasmonic semiconductor quantum SERS probe as a pathway for in vitro cancer detection, Nat. Commun. 9 (2018) 3065.

[5] E. D. Feng, T. T. Zheng, X. He, J. Q. Chen, Y. Tian, A novel ternary heterostructure with dramatic SERS activity for evaluation of PD-L1 expression at the single-cell level, Sci. Adv. 4 (2018) eaau3494.

[6] J. Lin, J. Yu, O. U. Akakuru, X. Wang, B. Yuan, T. Chen, L. Guo, A. Wu, Low temperature-boosted high efficiency photo-induced charge transfer for remarkable SERS activity of ZnO nanosheets, Chem. Sci. 11 (2020)9414.

[7] T. Man, W. Lai, C. Zhu, X. Shen, W. Zhang, Q. Bao, J. Chen, Y. Wan, H. Pei, L. Li, Perovskite mediated vibronic coupling of semiconducting SERS for biosensing, Adv. Funct. Mater. 32 (2022) 2201799.

[8] H. Fang, C. X. Zhang, L. Liu, Y. M. Zhao, H. J. Xu, Recyclable three-dimensional Ag nanoparticle-decorated TiO2 nanorod arrays for surface-enhanced Raman scattering, Biosens. Bioelectron. 64 (2015) 434.

[9] J. Lin, Y. Shang, X. Li, J. Yu, X. Wang, L. Guo, Ultrasensitive SERS Detection by Defect Engineering on Single Cu_2O Superstructure Particle, Adv. Mater.29 (2017) 1604797.

[10] X. T. Wang, W. X. Shi, Z. Jin, W. F. Huang, J. Lin, G. S. Ma, S. Z. Li, L. Guo, Remarkable SERS activity observed from amorphous ZnO nanocages, Angew. Chem. Int. Ed. 56 (2017) 9851.

[11] Z. Yu, W. L. Yu, J. Xing, R. A. Ganeev, W. Xin, J. L. Cheng, C. L. Guo, Charge Transfer Effects on Resonance-Enhanced Raman Scattering for Molecules Adsorbed on Single-Crystalline Perovskite, ACS Photonics. 5 (2018) 1619.

[12] D. Liu, W. Yi, Y. Fu, Q. Kong, G. Xi, In Situ Surface Restraint-Induced Synthesis of Transition-Metal Nitride Ultrathin Nanocrystals as Ultrasensitive SERS Substrate with Ultrahigh Durability, ACS Nano.16 (2022) 13123.